

Challenge and solution of characterizing glass transition temperature for conjugated polymers by differential scanning calorimetry

Zhiyuan Qian¹, Luke Galuska¹, William W. McNutt², Michael U. Ocheje³, Youjun He⁴, Zhiqiang Cao¹, Song Zhang¹, Jie Xu⁵, Kunlun Hong^{4,6}, Renée B. Goodman³, Simon Rondeau-Gagné³, Jianguo Mei², Xiaodan Gu1*

- 1. School of Polymer Science and Engineering, Center for Optoelectronic Materials and Devices, The University of Southern Mississippi, Hattiesburg, MS, 39406, USA
- 2. Department of Chemistry, Purdue University, West Lafayette, Indiana 47907, USA
- 3. Department of Chemistry and Biochemistry, University of Windsor, Windsor, Ontario, N9B3P4, Canada
- 4. Center for Nanophase Materials Sciences, Oak Ridge National Laboratory, Oak Ridge, Tennessee 37831, USA
- 5. Naonotechnology and Science Division, Argonne National Laboratory, Lemont, IL 60439, USA
- 6. Department of Chemical and Biomolecular Engineering, University of Tennessee, Knoxville, TN, 37996

Correspondence to: Xiaodan Gu (E-mail: xiaodan.gu@usm.edu)

((Additional Supporting Information may be found in the online version of this article.))

ABSTRACT

Thermomechanical properties of polymers highly depend on their glass transition temperature (T_g) . Differential scanning calorimetry (DSC) is commonly used to measure $T_{\rm g}$ of polymers. However, many conjugated polymers (CPs), especially donor-acceptor conjugated polymers (D-A CPs), do not show a clear glass transition when measured by conventional DSC. In this work, we discuss the origin of the difficulty for measuring T_g in such type of polymers. The changes in specific heat capacity (Δc_p) at T_g were accurately probed for a series of CPs by DSC. The results showed a significant decrease in Δc_p from flexible polymer (0.28 J·g⁻¹K⁻¹ for polystyrene) to rigid CPs (10⁻³ J·g⁻¹K⁻¹ for a naphthalene diimide-based D-A CP). When a conjugation breaker unit (flexible unit) is added to the D-A CPs, we observed restoration of the Δc_p at T_g by a factor of 10, confirming that backbone rigidity reduces the Δc_p . Additionally, an increase in the crystalline fraction of the CPs further reduces Δc_p . We conclude that the difficulties of determining T_g for CPs using DSC is mainly due to rigid backbone and semicrystalline nature.

INTRODUCTION

With unique chemically tunable electronic and optical properties, conjugated polymers (CPs), which are lightweight, flexible and deformable, have drawn significant interest.¹⁻ ⁶ Most of researches are focused on improving the

mobility, charge optical bandgap, processability by engineering chemical structures of conjugated polymers.⁷⁻⁹ However, there is a lack of understanding of their thermo-properties, such as glass transition temperature (T_g) for CPs, especially for donor-acceptor polymers (D-A



CPs) that possess record breaking device performance. 10,11 $T_{\rm g}$ is an important physical parameter that determines the processing condition and end-use temperature of a given polymeric material. When a polymer goes through the glass transition, its modulus can vary by $2{\sim}3$ orders of magnitude, dropping from GPa level for glassy state to MPa level for viscoelastic state. 12,13

For flexible or deformable electronics, it is desired to have a low modulus close to KPa range to match the modulus of human skin, hence, soft CPs with $T_{\rm g}$ lower than room temperature are preferred. In addition, the common practice in device fabrication requires an annealing process after depositing a polymer film, to facilitate ordered morphology and improve the charge transport mobility. 1 Such process needs to be carried out at a temperature above $T_{\rm g}$ to accelerate molecular dynamics. Additionally, operating devices above its $T_{\rm g}$ would cause change in the device morphology and potentially cause performance degradation over time. 14-16 As such, it is important to know the $T_{\rm g}$ of the conjugated polymers.

Our recent review has briefly summarized several experimental techniques which have been used to measure the T_g for thin film of CPs, including differential scanning AC-chip calorimetry (DSC), calorimetry, dynamic mechanical analysis (DMA), etc.¹⁷ Among them, AC-chip and DMA are quite successful in measuring T_g of D-A CPs, ^{18,19} whereas DSC, which has been widely used in non-conjugated and flexible polymers, often fails to detect T_g of D-A CPs even with adequate sample mass. 20,21 (T_g discussed herein refers to backbone $T_{\rm g}$.) For example, it has been shown that for diketopyrrole-based (DPP) polymers, neither conventional DSC nor Flash DSC exhibits a clear $T_{\rm g}$. ²²⁻²⁵

In the current work, we discuss the potential origin of complexity for measuring $T_{\rm g}$ for D-A CPs by DSC. We studied the specific heat capacities ($c_{\rm p}$) of several CPs, both conventional and D-A CPs, including poly(3-hexylthiophene) (P3HT) and poly(3-(4'-methylpentyl)thiophene) P3(4MP)T,

diketopyrrolopyrrole-based (DPP) naphthalene diimide-based (NDI) polymers, with standard sapphire reference method²⁶ using conventional DSC (Mettler Toledo DSC 3+ with FRS 6+ sensor). This measurement follows an ASTM international standard method for determining the specific heat capacity of a given material as a function of temperature. The methodology will be discussed in detail in the following experimental section. The specific heat capacity change between glass state and liquid state ($\Delta c_p = c_{p,l} - c_{p,g}$, 1 and g refer to liquid state and glassy state) at T_g for each material is obtained and compared with that for polystyrene (PS), a physical model polymer. The results show that Δc_p of CPs is at least one order of magnitude smaller than that of PS. We hypothesize that there are two reasons for the decrease in Δc_p . First, increased conjugation with large aromatic rings in the polymer backbone resulted in high backbone rigidity yielding minimal a conformation change above and below the T_{g} . We tested our hypothesis by designing a flexible alkyl conjugation-break linker (CBL) to restore backbone flexibility, thus enhancing the Δc_p . Second, semicrystalline nature restricts the amount of amorphous phase presented in the film, thus reducing the T_g signal which is dependent on amorphous phase content. We used flash scan DSC (Mettler Toledo Flash DSC 2+) investigate the effect of crystallinity on Δc_p , which dropped substantially with the increased degree of crystallinity. We end this work by providing several potential ways to improve the accuracy of measuring $T_{\rm g}$ of D-A CPs.

EXPERIMENTAL

Materials:

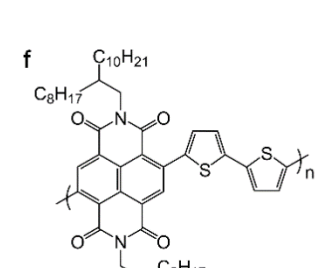
Chemical Structures of the materials investigated in the current work is shown in Figure 1.

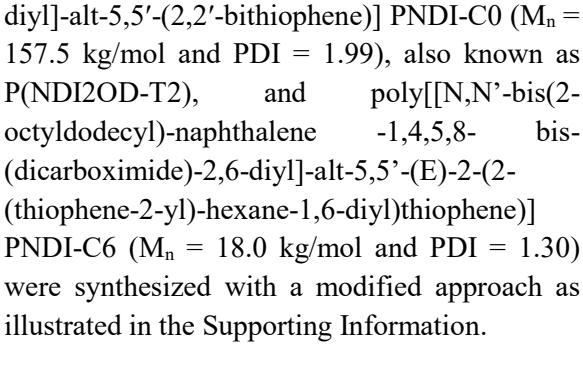
Polystyrene (PS) (number average molecular weight M_n of 173 kg/mol and PDI of 1.06, Polymer Source, Inc.) and regioregular (rreg) poly(3-hexylthiophene) (P3HT) (Sigma-Aldrich, regioregularity ~ 92%, M_n = 24.7 kg/mol

and PDI = 2.52) were purchased and used as received.

R-reg poly[3-(4'-methylpentyl)thiophene] P3(4MP)T ($M_n = 20.5 \text{ kg/mol}$ and PDI = 1.51) and poly [3-(2'-ethylbutyl)thiophene] P3(2EB)T ($M_n = 14.1 \text{ kg/mol}$ and PDI = 1.53) were synthesized by a modified GRIM method as reported in the literature. 27-30 2-Bromo-3-alkylthiophenes will react with Grignard Reagent (2, 2, 6, 6-Tetramethylpiperidinylmagnesium chloride lithium chloride complex solution) to give 2-Bromo-5-magnesiumchloridelithiumchloride-3-alkylthiophenes. The polymers have very high regularities of over 97%.

Poly[[N,N'-bis(2-octyldodecyl)-naphthalene-1,4,5,8-bis-(dicarboximide)-2,6-





Poly[diketopyrrolopyrrole-co-terthiophene] PDPP-T3 ($M_n = 27.0 \text{ kDa}$ and PDI = 3.2) was synthesized as reported in the literature.³¹ Molecular weight and PDI were estimated from high-temperature GPC (EcoSEC, Tosoh Bioscience) at 200°C in 1,2,4-trichlorobenzene calibrated by monodisperse polystyrene standards.

Figure 1. Chemical structures of the conjugated polymers investigated: (a). PS, (b). P3HT, (c). P3(4MP)T, (d). P3(2EB)T, (e). PDPP-T3, (f). PNDI-C0, (g). PNDI-C6.

Ċ₁₀H₂₁

Measurements:

Specific heat capacity

The specific heat capacity (c_p) measurements of PS, P3HT, P3(4MP)T, PDPP-T3, PNDI-C0, and PNDI-C6 were performed with the Sapphire method by following ASTM E1269-11²⁶ on Mettler-Toledo DSC 3+. Dry nitrogen purge gas at a flow rate of 20 ml/min was

applied during the tests. The instrument was calibrated with indium. The sapphire disc standard (ME51140818) was purchased from Mettler-Toledo. The mass of DSC pans utilized in the measurements were within \pm 0.01 mg to improve the accuracy. The sample mass was between $10\sim20$ mg. The measurement for each material composes three separate tests: blank scan, sapphire standard scan, and sample scan, with the same temperature program. A

heating/cooling rate of 10 K/min was employed, and the heat-cool-heat temperature range varied with the sample. (The scope of current work focuses on the backbone $T_{\rm g}$. Hence, the DSC temperature profile was not cover the side chain glass transition region, which typically occurs below -40 °C.¹⁷) The heat flow of second heating scan of sapphire and sample were corrected by subtracting the baseline (blank scan). After correction, the $c_{\rm p}$ of the sample was calculated with the following equation:

$$c_{p,s} = \frac{\dot{Q}_s \cdot m_{sap}}{\dot{Q}_{sap} \cdot m_s} c_{p,sap} \tag{1}$$

where \dot{Q} and m are the corrected heat flow and specimen mass, subscript s and sap stand for sample and sapphire, respectively. The value of $c_{p,sap}$ at a given temperature was obtained from the literature report.³²

Isothermal crystallization measurement

The isothermal crystallization measurements of P3(2EB)T were performed on Mettler-Toledo Flash DSC 2+. The MultiSTAR UFS 1 sensor was conditioned and corrected prior to the measurements. The bulk sample was then cut into small piece with a scalpel under the microscope and then transferred to the active heating area on the MultiSTAR UFS 1 sensor with an animal hair. A pre-melting step was performed to ensure good thermal contact between sample and sensor membrane. A high heating/cooling rate of 1000 K/s was employed to ensure the material reaches the disordered supercooled state during cooling and increase the signal-noise ratio. The measurements were carried out with the following temperature program: first, sample was heated to 250 °C, which is above the melting temperature, and held for 1 ms; then the sample was cooled down to the crystallization temperature of 90 °C, and held there for different times to allow the sample to crystallize; after that, the sample was cooled down to -20 °C and then reheated to 250 °C. The data analysis was performed on the reheating

Modified dynamic mechanical analysis (DMA)

Modified DMA measurements were performed on PNDI-C0 by solution casting the sample on glass fiber. The coated glass fiber then measured on a TA Instruments Q800 DMA under strain-controlled mode. A temperature ramp with heating rate of 3 K/min and frequency of 1 Hz was conducted. The strain was in the linear regime.

Solution X-ray scattering

Solution X-ray scattering was performed at Stanford Synchrotron Radiation Lightsource (SSRL) under beamline 4-2 at 15 keV. Samples were prepared at 5 mg/ml concentration in chlorobenzene at ambient conditions and allowed to dissolve overnight. Capillary based flow cells were utilized to mitigate the effect of capillary thickness and curvature on background scattering for accurate subtraction of solvent and capillary. Neat anhydrous chlorobenzene solvent was measured prior to each conjugated polymer solution for background subtraction. Each scattering experiment was performed at room temperature and run for 5 minutes for an adequate signal to noise ratio. And subsequently analyzed using SasView fitting software.

RESULTS AND DISCUSSION

First, we discuss the methodology we used to accurately determine the Δc_p . Sapphire method determines the cp of a sample by calibrating the sample heat flow signal with the signal of sapphire standard which has known cp (shown in Figure S1).²⁶ For the c_p curve of a sample, when a step change in c_p can be readily observed, the temperature range of glassy state and liquid state was then determined and fitted with two different straight lines, respectively. Then we calculate T_g and Δc_p . For example, in the case of PS, the glassy range and liquid range can be readily determined with an obvious step change, as shown in Figure 2a. We first obtained the Δc_p of PS and compared to the literature value. Then $T_{\rm g}$ was calculated based on the half-step method33 or Moynihan method34 depending on each specific case. In the case where glass transition region cannot be readily defined, a second technique, such as DMA, was conducted



to get a rough estimate of T_g . After that, based on one of the signatures of glass, enthalpy overshoot,³⁵ which happens when heating up an aged glass or in the case where the cooling rate/heating rate ratio less than 1, a physical aging experiment (temperature program schematically shown in Figure S2a) or cooling rate experiment was performed on DSC to confirm the glass transition region, and Δc_p was then determined. More detailed discussions are presented subsequently.

We performed the measurements on four CPs (P3HT, P3(4MP)T, PDPP-T3, PNDI-C0) and plotted c_p as a function of temperature in Figure 2. (Due to the scope of the current work, we limit our discussion herein on the temperature range at the vicinity of the glass transition. DSC heating scans in the full temperature range are provided in Figure S3 in Supporting Information. All CPs are semicrystalline since they all show a melting peak upon heating to high temperature. As expected, the glass transition of PS can be readily observed together with a typical enthalpy relaxation peak in Figure 1a. The $T_{\rm g}$ of PS determined by Moynihan method³⁴ is 99.0 °C. We obtained Δc_p at T_g by calculating the difference between the extrapolated liquid line and glass line, which gives a value of 0.28 J·g⁻¹K⁻¹ and has a good agreement with the literature report value of 0.28~0.30 J·g⁻¹K⁻¹.^{36,37}

Turning to the CPs, we observed a much weaker glass transition both for P3HT and P3(4MP)T, as shown in Figure 2b and 2c, respectively. For P3HT, it features a two-step transition where the first step with a T_g of 11.7 °C (this value shows great agreement the literature reported value of 12~14 °C measured with DSC and DMA.^{15,38-41}) is associated with the mobile amorphous fraction (MAF) and the second one with a $T_{\rm g}$ of 42.2 °C is related to the rigid amorphous fraction (RAF). This is consistent with previous work by Remy et al.⁴² Upon tuning chain isomerism, side surprisingly, P3(4MP)T only gives a one-step transition with a $T_{\rm g}$ of 35.2 °C. Such a difference is presumably

the difference in crystalline related to morphology and requires further investigation in future. The comparison of Δc_p at T_g among PS, P3HT and P3(4MP)T is depicted in Figure 2f, in which we see a much smaller Δc_p for P3HT isomers (0.067 J·g⁻¹K⁻¹ for P3HT and 0.045 J·g⁻¹ ${}^{1}K^{-1}$ for P3(4MP)T). Such a small Δc_p for r-reg P3HT and P3(4MP)T herein is presumably related to rigid backbone, and semicrystalline nature. We will discuss the effects of backbone rigidity (in terms of persistence length) and crystallinity (in terms of relative degree of crystallinity) on Δc_p in more detail in the following section.

DSC measurements for PDPP-T3 and PNDI-C0, which have highly planar and rigid backbone structures, are presented in Figure 2d and 2e, the step change in c_p, thus the glass transition, cannot be readily seen from the DSC scans. A linear curve is observed and is expected based on various previous reports.^{21-24,43-47} PDPP-T3 shows a small curvature at the vicinity of 0 °C. Zhang et al. recently reported a T_g of ~ 20 °C both from AC-Chip calorimetry and modified DMA.¹⁹ In general, the $T_{\rm g}$ obtained from AC-Chip and DMA is 10~20 °C higher than that from conventional DSC.¹⁸ Hence, the slight change in slope near 0 °C in Figure 2d is related to the glass transition of the PDPP-T3 backbone. We further conformed this by performing the physical aging experiments (see temperature profile Figure S2b), where sample was purposely aged at 0 °C, -5 °C, and -10 °C, respectively, for 60 min before reheating up. The resultant DSC heating scans are plotted in Figure S4a and enthalpy overshoots resulted from structure recovery were observed in all three aging temperatures. We then estimated its Δc_p from the baseline subtracted apparent c_p curve, which is approximately 0.013 J·g⁻¹K⁻¹ with a T_g of ~ 2.2 °C, as presented in Figure S4b. For PNDI-C0, we could not determine the exact value of Δc_p . The value is expected to be lower than PDPP-T3, on the order of 10^{-3} J·g⁻¹K⁻¹ or smaller, owing to the almost linearly increased cp over the temperature range we investigated.



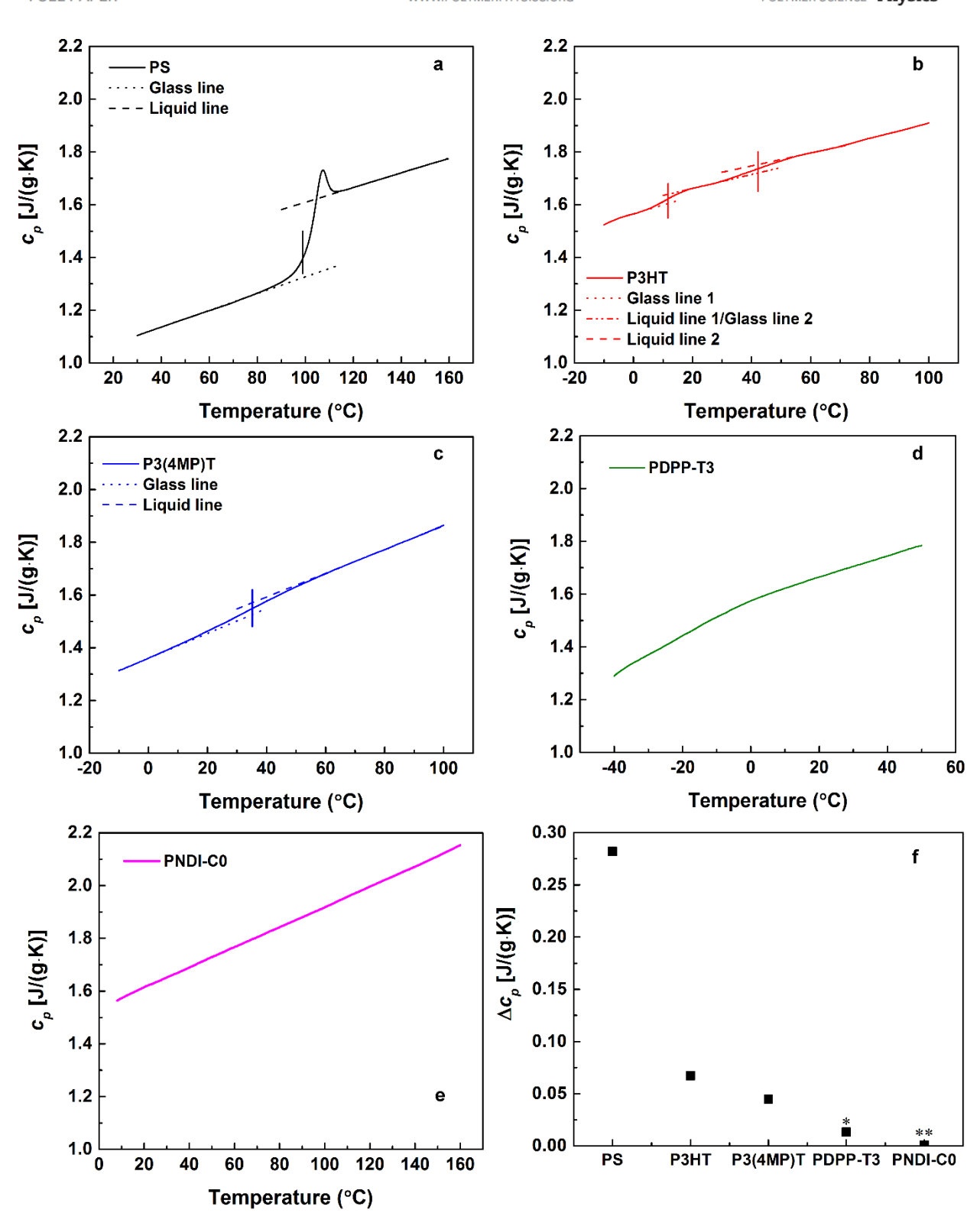


Figure 2. Specific heat capacities (solid line) of (a). PS, (b). P3HT, (c). P3(4MP)T, (d). PDPP-T3, and (e). PNDI-C0 obtained from the Sapphire method using a conventional DSC with 10 K/min heating/cooling rate (Second heating scans were used for data analysis.). The dotted line and dash lines are the glass line and liquid line, respectively, to determine $T_{\rm g}$ and heat capacity change $\Delta c_{\rm p}$ at $T_{\rm g}$. The vertical lines in (a),



(b) and (c) mark the position of T_g . (f). The heat capacity change Δc_p at T_g for PS, P3HT and P3(4MP)T. Δc_p of P3HT is the total change of the two-step transition. * Data estimated from apparent c_p curve in Figure S3b. ** Estimated value based on the curvature difference in part (d) and (e).

Effect of backbone rigidity

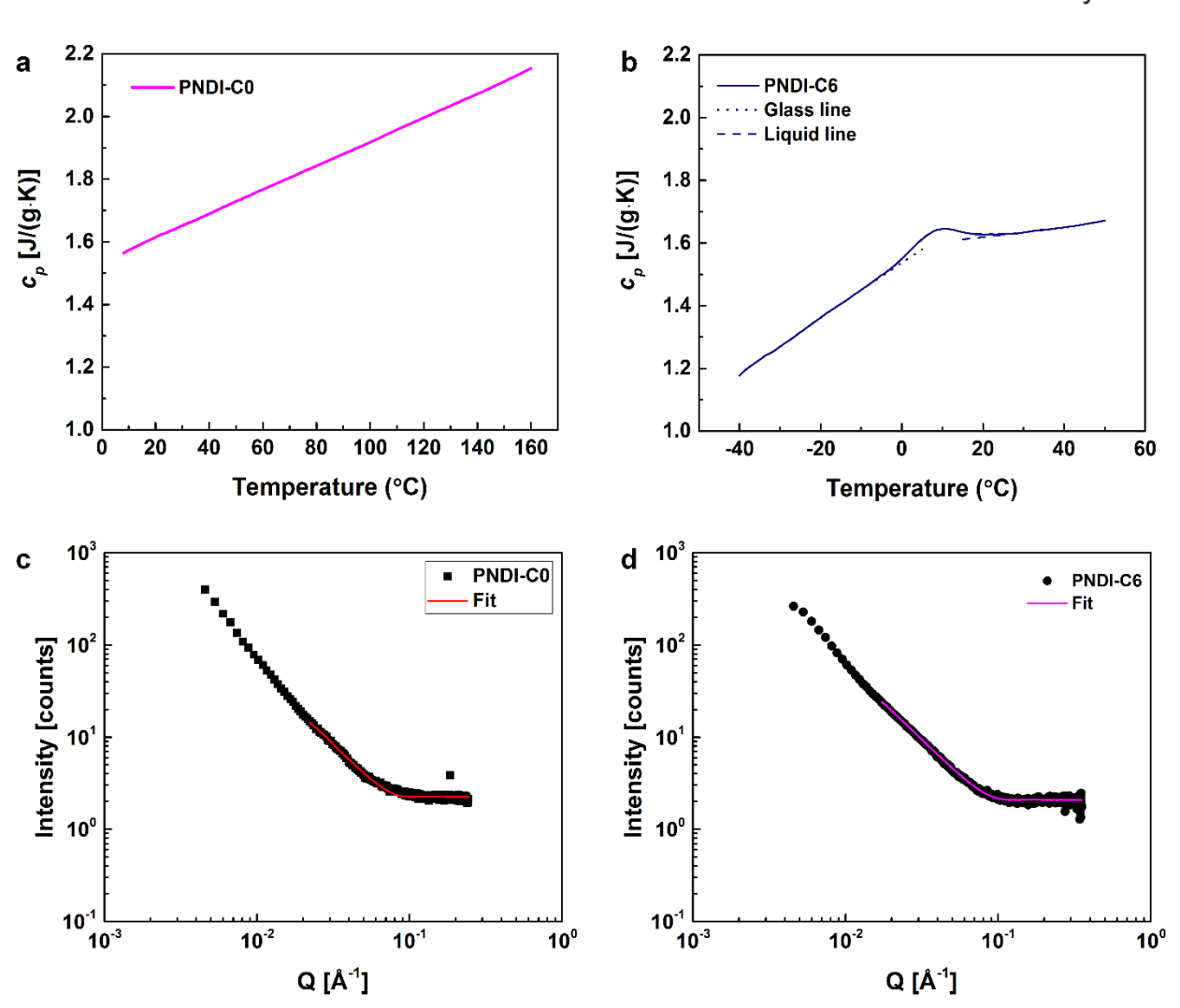
Based on our experimental findings, we hypothesize that the increase in backbone rigidity causes a drop in the Δc_p . For example, it has been reported for poly(n-alkyl methacrylate)s, with the increase of n-alkyl side chain length, the persistence length (l_p) increases, i.e., backbone becomes more rigid. 48,49 Meanwhile, a decrease in Δc_p is observed as side chain length increases.⁵⁰ In the case of P3HT, r-reg P3HT has a more rigid backbone (lp of 2.9 nm) compared with regiorandom (r-ran) P3HT (l_p of 0.9 nm)^{15,51} and PS $(l_p \text{ of } 0.7 \text{ nm})$, 52,53 as shown above, a significant decrease in Δc_p is observed. (It has been reported that r-ran P3HT, which is amorphous and more flexible, gives a Δc_p of approximately 0.3 J·g⁻¹K⁻¹, ^{42,54} which is close to the value of PS.) Same argument is applicable to P3(4MP)T, which has a l_p of approximately 2~2.5 nm,⁵⁵ similar to that of r-reg P3HT. While for DPP-based D-A CPs, they tend to have even large l_p than r-reg P3HT due to more rigid backbone.⁵⁶ Hence, we see a much smaller Δc_p for PDPP-T3.

Such hypothesis was tested engineering D-A CPs with different backbone rigidity by introducing flexible alkyl conjugationbreak linker (CBL) into the D-A CPs (Chemical structure shown in Figure 1g) and measuring Δc_n We measured both PNDI-C0 (fully conjugated) and PNDI-C6 (with non-conjugated flexible segment) and studied the effect of the conjugation breaker on $T_{\rm g}$ (Figure 3) as well as the backbone rigidity (Figure S7). The glass transition region

became more obvious (Figure 3b) when a 6carbon CBL was incorporated to the backbone repeating unit of PNDI-C0 (Figure 3a). The $T_{\rm g}$ of PNDI-C6 was determined to be -0.1 °C with a Δc_p of 0.052 J·g⁻¹K⁻¹, which is in the same range as P3HT and P3(4MP)T, and at least one order of magnitude greater than the Δc_p of fully conjugated PNDI-C0. The glass transition region of PNDI-C6 was confirmed with the physical aging and cooling rate dependence experiments. In both cases, enthalpy overshoot is observed on heating scans, as shown in Figure S5.

The reduction in backbone rigidity with presence of CBL was verified through solution small angle X-ray scattering (SAXS) for polymers dissolved in chlorobenzene. Modeling of the scattering data enabled approximate persistent lengths to be determined. In our case, the polymer aggregation presented at the room temperature prohibits reliable quantitative data fitting in the low scattering vector region near the beam stop. We used the flexible cylinder model, a model that generally used to fit semi-rigid polymer, to fit the solution scattering data, as shown in Figures 3c and 3d.57 The raw data of solution scattering are shown in Figure S6. The fitting parameters are listed in Table S1. With the flexible cylinder model, we estimate a 40% reduction in l_p upon introducing flexible alkyl chain to PNDI-C0. Future investigations at lower concentration and elevated temperatures are warranted to mitigate aggregation and elucidate the Guinear regime for precise quantitative analysis.





WWW.POLYMERPHYSICS.ORG

Figure 3. Restoration of Δc_p by reducing the backbone rigidity. The specific heat capacities (solid line) of (a). PNDI-C0 and (b). PNDI-C6 obtained from the Sapphire method with conventional DSC. The dotted line and dashed lines in (b) are glass line and liquid line, respectively. (In addition, we notice that surprisingly the glassy lines of PNDI-C0 and PNDI-C6 do not have same slope, which we do not know the exact origin at this point.) (c) and (d) are the solution X-ray scattering results and the flexible cylinder model fit for PNDI-C0 and PNDI-C6.

Effect of crystallinity

It has long been recognized that for conventional semicrystalline polymers, the glass transition phenomenon depends on the degree of crystallinity, including the width of glass transition region, $T_{\rm g}$ and $\Delta c_{\rm p}$. However, there is little work performed on understanding the effect of relative degree of crystallinity (RDOC) on the $T_{\rm g}$ of CPs due to experimental challenges associated with trapping samples into desired

RDOC. Experimentally, precisely controlling the RDOC for conjugated polymer is not straight forward. In general, the conventional DSC is not capable to quench the CPs to the supercooled, or completely amorphous state owing to the fast crystallization rate of conjugated polymers. ^{15,20,25,38,58-61} For example, as shown in Figure S7, the crystallization of P3(2EB)T is inevitable upon cooling it from its melt state with conventional DSC even at 100 K/min; while, faster cooling speed using flash DSC can trap

P3(2EB)T into the fully amorphous phase using a cooling rate of 60,000 K/min (1,000 K/s), as shown in Figure 4 subsequently. This trapped amorphous glass can be heated up to its crystallization temperature and vary isothermal crystallization time to precisely control the degree of crystallinity.

In this work, we demonstrated P3(2EB)T with different RDOC by varying the isothermal crystallization time at 90 °C after quenching it from the melt state. The temperature profile is schematically presented in Figure S8.62 The corresponding reheating scans are presented in Figure 4a, in which the area of the melting peak grows with the crystallization time and in the meantime the glass transition region broadens. We integrated the melting peak area near 160 °C (shown in Figure S9) and compared the RDOC (RDOC = A_t/A_{20000} , A_t is the peak area at crystallization time t). And the resultant normalized Δc_p is depicted in Figure 4b as a function of RDOC. As expected, a decrease in normalized Δc_p are observed with the increase of RDOC. When RDOC is above 0.2, the normalized Δc_p almost linearly decreases with RDOC (more crystalline domain, less entropy change during the glass transition). The relative change in Δc_p clearly shows a significant decrease for P3(2EB)T at high RDOC, which then explains the difficulty in obtaining $T_{\rm g}$ from conventional DSC for semicrystalline CPs. Meantime an elevation in T_g is observed as shown in supporting Figure S10.

In addition, since P3(2EB)T is able to be quenched into fully amorphous state with Flash DSC, the effects of chain rigidity and crystallization can be deconvoluted. Based on the

symmetric line analysis method, 63-67 we estimated the sample mass of P3(2EB)T in Flash DSC measurement to be approximately 67 ng. Hence, the $\Delta c_{p,am}$ at T_g for the fully amorphous P3(2EB)T is calculated to be approximately 0.14 J·g⁻¹K⁻¹, two times smaller than PS and r-ran P3HT (0.28~ 0.3 J·g⁻¹K⁻¹). (The procedures of the calculations are described in detail in Supporting Information and Figure S11.) In addition, the second heating curve of r-reg P3HT (Figure S3b) gives an enthalpy of fusion (ΔH_m) of 16 J/g, given that the enthalpy of fusion of perfect P3HT crystal (ΔH_m^{∞}) in the literature spans from 33 to 99 J/g, 68-76 we estimate that the absolute crystallinity $(X_c =$ $\Delta H_m/\Delta H_m^{\infty}$) of r-reg P3HT here should range from 16% to 49% depending on the value of ΔH_m^{∞} . Hence, the $\Delta c_{p,am}$ at T_g for the fully amorphous r-reg P3HT is estimated between 0.08 to 0.13 J·g⁻¹K⁻¹, which is in a similar range to that of r-reg P3(2EB)T. Besides, as r-reg P3(2EB)T, P3(4MP)T and P3HT are isomers, the l_p is presumably 2~3 nm. Recall that PS and r-ran P3HT possess a l_p of 0.7 nm and 0.9 nm, respectively, demonstrating higher flexibility than r-reg P3(2EB)T and r-reg P3HT, which corresponds well with the higher Δc_p of PS and rran P3HT. (We also performed the Flash DSC measurement on PDPP-T3 and PNDI-C0 with UFH 1 sensor. However, as shown in Figure S12, the crystallization during cooling is evitable even with cooling rate up to 10,000 K/s.) Recently, Yin et al. investigated the glass transition behavior for polymers of intrinsic microporosity, which are non-conjugated but also possess rigid backbone, low Δc_p of 0.16 J·g⁻¹K⁻¹ has been observed.⁷⁷ Therefore, this indicates a correlation between small Δc_p and rigid chain, or large Δc_p for flexible chain.



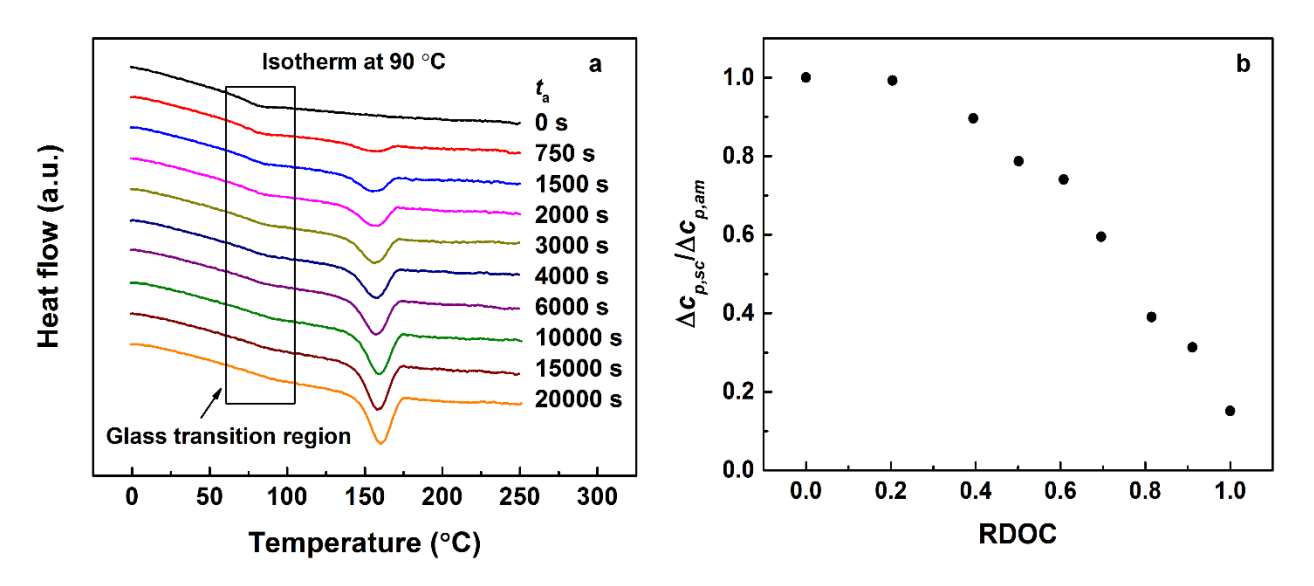


Figure 4. Controlled isotherm crystallization of CPs and its effect on glass transition (a). Reheating scans of P3(2EB)T after isothermal crystallization at 90 °C for different times (as indicated in the legend) measured with flash DSC. (b). Apparent $\Delta c_{p,sc}$ at T_g for P3(2EB)T at different relative degrees of crystallinity (RDOC) normalized by the apparent $\Delta c_{p,am}$ at fully amorphous state.

Based on the results present above, we see that D-A CPs in general possess a low Δc_p at $T_{\rm g}$ (more than one order of magnitude smaller than PS), which limits the application of conventional DSC in measuring T_g . This is presumably owing to the following three factors: rigid backbone, semicrystalline nature and high side chain content. 1) In order to improve the electrical performance, D-A CPs are designed in a way which have highly planar and rigid backbone to facilitate high charge transport mobility. Typically, high backbone rigidity reduces the entropy of the chain confirmation near the glass transition. 2) Many D-A CPs are semicrystalline. In general, the crystallization rate of D-A CPs is high compared with the cooling rate of a conventional DSC, i.e., it is difficult to melt D-A CPs and quench them into a fully amorphous state. Since only amorphous fraction contributes to T_g , Δc_p is then further reduced. Hence, the overall contributions lead to a low Δc_p . 3) High mass fraction of long and branched flexible side chains are commonly used in the CPS to improve the solubility issue. Meanwhile, it has been suggested for nonconjugated polymers, introducing bulky side chains lead to high glassy-state entropy and glassy-state c_p , while the liquid c_p is not affected,

which then results in a low Δc_p at T_g . Same argument is presumably applicable to D-A CPs.

Remedy of measuring T_g for D-A CPs with extremely low Δc_p

The data presented in Figures 1 and 2 suggest that for a D-A CP with Δc_p lower than 0.01 J·g⁻¹K⁻¹, DSC cannot readily measure its T_g even with adequate sample mass (e.g. tens of milligrams). In this scenario, a secondary measurement is recommended to compliment the DSC measurement to locate T_g . AC-Chip and DMA are also widely used to obtain $T_{\rm g}$ by measuring the material dynamics, which do not rely on the magnitude of Δc_p . Though AC-Chip has a higher sensitivity, it is not readily available for most research groups. In the case of modified DMA, it cannot obtain the absolute moduli due to unspecified sample geometry when supported by another substrate and this might cause difficulty in distinguishing glass transition phenomenon with various other phase transitions (e.g. melting, liquid crystalline transition) in CPs.⁷⁹ In addition, since several thermal transitions exhibit a peak in tanδ response, which potentially introduces challenges to accurately measure T_g . Therefore, we suggest combining the modified DMA herein with DSC to help unravel the missing $T_{\rm g}$.

This methodology is rather simple. One first roughly estimate the potential temperature range for glass transition from DMA, followed by a physical aging measurement or cooling rate dependence measurement on DSC to confirm the $T_{\rm g}$ of CPs. The design of such methodology is based on one signature of glass, i.e., enthalpy overshoot,35 which is a phenomenon long been recognized for glass. When a material is cooled from equilibrium state, the mobility decreases until it is not long able to maintain the equilibrium at given experimental time scale. As a result, glass transition takes place, and material goes to the glassy state, which is in the nonequilibrium The resultant enthalpy change schematically shown in Figure S13. Due to the excess enthalpy in the glassy state compared with equilibrium state, the material has a tendency to relax toward the equilibrium. This process is known as physical aging or structure recovery. In this case, when an aged sample is reheated up, the response evolves parallelly to the glassy line. As it crosses the equilibrium line, due to the lower mobility compared with unaged sample, the response cannot follow the heating rate and leads to an overshoot in enthalpy. As the temperature being further increased, the material is finally mobile enough to follow the heating rate and reach to the equilibrium state.³⁵ Similarly, when a slow cooled sample is fast heated, since it relaxes more during cooling, an enthalpy overshoot also appears on the heating curve. Figures S14a and S14b plot the heat flow curves of PS obtained from physical aging experiments⁸⁰ and cooling rate dependence experiments.⁸¹ It is readily seen that apart from the glass transition region, in which the enthalpy overshoot occurs, the glass lines and liquid lines for the aged run and unaged run well overlap on top of each other. This is also true for the heating scans in the cooling rate experiments. Hence, we can use these two experiments to improve the accuracy of locating the glass transition region, glass line and liquid line. (We remark here that there are different half-step,³³ Moynihan method,³⁴ methods, inflection point, 82 to obtain $T_{\rm g}$ value from DSC scans. Regardless, cooling rate dependence and aging experiments are highly recommended for verifying the validity of T_g, especially for material with extremely low Δc_p .)

Here, we use PNDI-C0 as an example to illustrates what can be done to probe the CPs with weak $T_{\rm g}$. Although a direct heating scan on DSC does not show any sign of T_g (Figure 1e), careful experimental design based on the signature of glass transition, which is enthalpy relaxation, can be utilized to reveal the glass transition region on DSC. Enthalpy relaxation in the heating scan is a result of structure recovery. It normally appears in following two cases: 1) when cooling rate is lower than heating rate and 2) when heating up an aged sample. We have demonstrated the enthalpy relaxation in Figures S3 and S5 for PDPP-T3 and PNDI-C6, both have Δc_p larger than NDI-C0, which is easy to measure. This physical aging experiment could also work on PNDI-C0, and we performed the aging experiment for PNDI-C0 at 70 °C. We first roughly estimated the $T_{\rm g}$ for PNDI-C0 using DMA results of PNDI-C0 thin film as shown in Figure S15a. A peak in tanδ appears at 137.21 °C, which is presumably the T_g associated with the backbone motion of the PNDI-C0. Figure S15b plots the comparison of DSC scans between unaged and aged conditions, in which an enthalpy overshoot is observed in the temperature range of approximately 80 to 120 °C. We estimated the T_g from the unaged condition, which gives approximately 101.9 °C with apparent Δc_p of approximately $2.4 \times 10^{-3} \text{ J} \cdot \text{g}^{-1} \text{K}^{-1}$.

CONCLUSIONS

In summary, the glass transition of a series of CPs, including conventional thiophene based CPs (P3HT and P3(4MP)T) and D-A CPs (DPP-T3, PNDI-C0 and PNDI-C6), was investigated with DSC. AMST E1269-11 method using sapphire as reference sample was employed to measure c_p. In addition, flash DSC measurements were conducted on P3(2EB)T to establish the effect of crystallinity on Δc_p , where Δc_p exhibits significant decrease as crystallinity increases. The results show that CPs possess a much lower Δc_p compared with PS (0.28) J·g⁻¹K⁻¹), especially for D-A CPs, which can be as low as in the order of 10^{-3} J·g⁻¹K⁻¹. Such low Δc_p is mainly owing to the rigid



backbone and high side chain content as well as semicrystalline nature, which explains the missing $T_{\rm g}$ often observed in DSC curves. We also proposed to combine the modified DMA experiments with the physical aging experiments on DSC to improve the accuracy of measuring $T_{\rm g}$, which is found to be successful even for the D-A CPs with $\Delta c_{\rm p}$ of 10^{-3} J·g⁻¹K⁻¹.

ACKNOWLEDGEMENTS

This work is supported by the U.S. Department of Energy, Office of Science, Office of Basic Energy Science under award number of DE-SC0019361 for Z.Q., Z.C. and X.G. S.Z. also acknowledge NSF for partial supported through office of integrative activities (OIA) by NSF OIA-1757220. L.G. thanks NSF NRT for providing support with grant #1449999. W.M. and J.M. acknowledge NSF grant #1653909 for the support of conjugated polymer synthesis. S.R.-G. thank the Natural Sciences and Engineering Research Council of Canada (NSERC) for financial support (RGPIN-2017-06611 and NETGP-508526-17). M.U.O. thank NSERC for a doctoral scholarship. R.G.B. thank NSERC for an undergraduate student research award. Part of the polymers were synthesized at the Center for Nanophase Materials Sciences, which is a DOE Office of Science User Facility. J.X. acknowledges the Center for Nanoscale Materials, a U.S. Department of Energy Office of Science User Facility, and supported by the U.S. Department of Energy, Office of Science, under Contract No. DE-AC02-06CH11357. Use of the Stanford Synchrotron Radiation Lightsource, SLAC National Accelerator Laboratory, is supported by the U.S. Department of Energy, Office of Science, Office of Basic Energy Sciences under Contract No. DE-AC02-76SF00515. The instrument used in this work flash DSC was acquired with support from ERDC. We would like to thank Eric King at The University of Southern Mississippi for assisting on the NMR measurement on P3HT and GPC measurement on P3HT and PNDI-C0. We would like to thank Dr. Brian N. Turner from MettlerToledo, Inc. and Madhusudhan R. Pallaka at Texas Tech University for the great discussion about Sapphire method, Matthew Hartline at The University of Southern Mississippi for conforming the $T_{\rm g}$ of PS with TA Instruments DSC Q200. We would like to thank Guorong Ma at The University of Southern Mississippi for assisting on the absolute heat capacity measurement of P3(2EB)T.

REFERENCES

1.Xu, J.; Wu, H.-C.; Zhu, C.; Ehrlich, A.; Shaw, L.; Nikolka, M.; Wang, S.; Molina-Lopez, F.; Gu, X.; Luo, S.; Zhou, D.; Kim, Y.-H.; Wang, G.-J. N.; Gu, K.; Feig, V. R.; Chen, S.; Kim, Y.; Katsumata, T.; Zheng, Y.-Q.; Yan, H.; Chung, J. W.; Lopez, J.; Murmann, B.; Bao, Z. *Nat. Mater.* **2019**, 1.

2.Chortos, A.; Bao, Z. *Mater. Today* **2014**, *17*, 321.

3. Someya, T.; Bao, Z.; Malliaras, G. G. *Nature* **2016**, *540*, 379.

4.Wang, S.; Xu, J.; Wang, W.; Wang, G. J. N.; Rastak, R.; Molina-Lopez, F.; Chung, J. W.; Niu, S.; Feig, V. R.; Lopez, J.; Lei, T.; Kwon, S. K.; Kim, Y.; Foudeh, A. M.; Ehrlich, A.; Gasperini, A.; Yun, Y.; Murmann, B.; Tok, J. B.

H.; Bao, Z. *Nature* **2018**, *555*, 83. 5.Oh, J. Y.; Rondeau-Gagné, S.; Chiu, Y. C.;

Chortos, A.; Lissel, F.; Wang, G. J. N.;

Schroeder, B. C.; Kurosawa, T.; Lopez, J.;

Katsumata, T.; Xu, J.; Zhu, C.; Gu, X.; Bae, W. G.; Kim, Y.; Jin, L.; Chung, J. W.; Tok, J. B. H.; Bao, Z. *Nature* **2016**, *539*, 411.

6.Gu, X.; Shaw, L.; Gu, K.; Toney, M. F.; Bao, Z. *Nat. Commun.* **2018**, *9*, 534.

7. Yao, Y.; Dong, H.; Hu, W. Adv. Mater. **2016**, 28, 4513.

8. Sirringhaus, H. *Adv. Mater.* **2014**, *26*, 1319. 9. Yan, C.; Barlow, S.; Wang, Z.; Yan, H.; Jen, A. K. Y.; Marder, S. R.; Zhan, X. *Nat. Rev. Mater.* **2018**, *3*, 18003.

10.Meng, L.; Zhang, Y.; Wan, X.; Li, C.; Zhang, X.; Wang, Y.; Ke, X.; Xiao, Z.; Ding, L.; Xia, R.; Yip, H.-L.; Cao, Y.; Chen, Y. *Science* **2018**, *361*, 1094

11.Nikolka, M.; Nasrallah, I.; Rose, B.; Ravva, M. K.; Broch, K.; Sadhanala, A.; Harkin, D.;

- Charmet, J.; Hurhangee, M.; Brown, A.; Illig, S.; Too, P.; Jongman, J.; McCulloch, I.; Bredas, J.-L.; Sirringhaus, H. Nat. Mater. 2016, 16, 356. 12. Ferry, J. D. Viscoelastic Properties of Polymers: John Wiley & Sons, Inc., 1980. 13. Tobolsky, A. V. Properties and structure of polymers; John Wiley & Sons, Inc., 1960. 14. Gumyusenge, A.; Tran, D. T.; Luo, X.; Pitch, G. M.; Zhao, Y.; Jenkins, K. A.; Dunn, T. J.; Ayzner, A. L.; Savoie, B. M.; Mei, J. Science **2018**, 362, 1131 15. Müller, C. Chem. Mater. 2015, 27, 2740. 16.Lindqvist, C.; Sanz-Velasco, A.; Wang, E.; Bäcke, O.; Gustafsson, S.; Olsson, E.; Andersson, M. R.; Müller, C. J. Mater. Chem. A **2013**, *1*, 7174. 17.Qian, Z.; Cao, Z.; Galuska, L.; Zhang, S.; Xu, J.; Gu, X. Macromol. Chem. Phys. 2019, 1900062. 18. Zhang, S.; Ocheje, M. U.; Luo, S.; Ehlenberg, D.; Appleby, B.; Weller, D.; Zhou, D.; Rondeau-Gagné, S.; Gu, X. Macromol. Rapid Commun. 2018, 39, 1800092. 19. Zhang, S.; Ocheje, M. U.; Huang, L.; Galuska, L.; Cao, Z.; Luo, S.; Cheng, Y.-H.; Ehlenberg, D.; Goodman, R. B.; Zhou, D.; Liu, Y.; Chiu, Y.-C.; Azoulay, J. D.; Rondeau-Gagné, S.; Gu, X. Adv. Electron. Mater. 2019, 1800899. 20. Snyder, C. R.; DeLongchamp, D. M. Curr. Opin. Solid State Mater. Sci. 2018, 22, 41. 21. Wang, G.-J. N.; Molina-Lopez, F.; Zhang, H.; Xu, J.; Wu, H.-C.; Lopez, J.; Shaw, L.; Mun, J.; Zhang, Q.; Wang, S.; Ehrlich, A.; Bao, Z. *Macromolecules* **2018**, *51*, 4976. 22.Chen, S.; Sun, B.; Hong, W.; Aziz, H.; Meng, Y.; Li, Y. J. Mater. Chem. C 2014, 2, 2183. 23. Yu, H.; Park, K. H.; Song, I.; Kim, M.-J.; Kim, Y.-H.; Oh, J. H. J. Mater. Chem. C 2015, *3*, 11697. 24. Zhang, A.; Xiao, C.; Wu, Y.; Li, C.; Ji, Y.; Li, L.; Hu, W.; Wang, Z.; Ma, W.; Li, W. Macromolecules **2016**, 49, 6431. 25. Yang, S.-F.; Liu, Z.-T.; Cai, Z.-X.; Dyson, M. J.; Stingelin, N.; Chen, W.; Ju, H.-J.; Zhang, G.-X.; Zhang, D.-Q. Adv. Sci. 2017, 4, 1700048. 26.ASTM E1269-11. Standard Test Method for Determining Specific Heat Capacity by Differential Scanning Calorimetry: West
- 27. Masuda, N.; Tanba, S.; Sugie, A.; Monguchi, D.; Koumura, N.; Hara, K.; Mori, A. *Org. Lett.* **2009**, *11*, 2297.
- 28. Shunsuke, T.; Shota, T.; Youhei, O.; Hikaru, M.; Shuji, O.; Atsunori, M. *Chem. Lett.* **2011**, *40*, 398.
- 29.Tamba, S.; Shono, K.; Sugie, A.; Mori, A. *J. Am. Chem. Soc.* **2011**, *133*, 9700.
- 30. Tanaka, S.; Tamba, S.; Tanaka, D.; Sugie, A.; Mori, A. *J. Am. Chem. Soc.* **2011**, *133*, 16734. 31. Yi, Z.; Sun, X.; Zhao, Y.; Guo, Y.; Chen, X.; Qin, J.; Yu, G.; Liu, Y. *Chem. Mater.* **2012**, *24*, 4350.
- 32.Ditmars, D.; Ishihara, S.; Chang, S.; Bernstein, G.; West, E. *J. Res. Natl. Bur. Stand.* **1982**, *87*, 159.
- 33.ASTM E1356-08. Standard Test Method for Assignment of the Glass Transition Temperatures by Differential Scanning Calorimetry: West Conshohocken, PA, **2014**. 34.Moynihan, C. T.; Easteal, A. J.; De Bolt, M. A.; Tucker, J. *J. Am. Ceram. Soc.* **1976**, *59*, 12. 35.McKenna, G. B.; Simon, S. L. *Macromolecules* **2017**, *50*, 6333.
- 36.Qian, Z.; Koh, Y. P.; Pallaka, M. R.; Chang, A. B.; Lin, T.-P.; Guzmán, P. E.; Grubbs, R. H.; Simon, S. L.; McKenna, G. B. *Macromolecules* **2019**, *52*, 2063.
- 37. Gaur, U.; Wunderlich, B. J. Phys. Chem. Ref. Data 1982, 11, 313.
- 38.Zhao, Y.; Yuan, G.; Roche, P.; Leclerc, M. *Polymer* **1995**, *36*, 2211.
- 39.Zhao, J.; Swinnen, A.; Van Assche, G.; Manca, J.; Vanderzande, D.; Mele, B. V. *J. Phys. Chem. B.* **2009**, *113*, 1587.
- 40.Pankaj, S.; Beiner, M. J. Phys. Chem. B. **2010**, 114, 15459.
- 41.Bruner, C.; Novoa, F.; Dupont, S.; Dauskardt, R. *ACS Applied Materials & Interfaces* **2014**, *6*, 21474.
- 42.Remy, R.; Wei, S.; Campos, L. M.; Mackay, M. E. *ACS Macro Lett.* **2015**, *4*, 1051.
- 43.Gu, X.; Yan, H.; Kurosawa, T.; Schroeder, B. C.; Gu, K. L.; Zhou, Y.; To, J. W. F.;
- Oosterhout, S. D.; Savikhin, V.; Molina-Lopez, F.; Tassone, C. J.; Mannsfeld, S. C. B.; Wang, C.; Toney, M. F.; Bao, Z. *Adv. Energy Mater.* **2016**, *6*, 1601225.
- 44.Yao, J.; Yu, C.; Liu, Z.; Luo, H.; Yang, Y.; Zhang, G.; Zhang, D. *J. Am. Chem. Soc.* **2016**, *138*, 173.



Conshohocken, PA, 2018.

- 45.Schroeder, B. C.; Kurosawa, T.; Fu, T.; Chiu, Y.-C.; Mun, J.; Wang, G.-J. N.; Gu, X.; Shaw, L.; Kneller, J. W. E.; Kreouzis, T.; Toney, M. F.; Bao, Z. Adv. Funct. Mater. 2017, 27, 1701973. 46.Wang, G.-J. N.; Zheng, Y.; Zhang, S.; Kang, J.; Wu, H.-C.; Gasperini, A.; Zhang, H.; Gu, X.; Bao, Z. Chem. Mater. 2018. 47.Gasperini, A.; Wang, G.-J. N.; Molina-Lopez, F.; Wu, H.-C.; Lopez, J.; Xu, J.; Luo, S.;
- 4/.Gasperini, A.; Wang, G.-J. N.; Molina-Lopez, F.; Wu, H.-C.; Lopez, J.; Xu, J.; Luo, S.; Zhou, D.; Xue, G.; Tok, J. B. H.; Bao, Z. *Macromolecules* **2019**, *52*, 2476.
- 48.Xu, Z.; Hadjichristidis, N.; Fetters, L. J.; Mays, J. W. In Physical Properties of Polymers; Springer Berlin Heidelberg: Berlin, Heidelberg, 1995, 1.
- 49. Campbell, C. G.; Vogt, B. D. *Polymer* **2007**, *48*, 7169.
- 50.Donth, E. *J. Polym. Sci., Part B: Polym. Phys.* **1996**, *34*, 2881.
- 51.McCulloch, B.; Ho, V.; Hoarfrost, M.; Stanley, C.; Do, C.; Heller, W. T.; Segalman, R. A. *Macromolecules* **2013**, *46*, 1899.
- 52.Fetters, L. J.; Lohse, D. J.; Richter, D.; Witten, T. A.; Zirkel, A. *Macromolecules* **1994**, 27, 4639.
- 53.Hiemenz, P. C.; Lodge, T. P. Polymer Chemistry; CRC Press, Taylor & Francis Group: Boca Raton, FL, **2007**.
- 54.Hugger, S.; Thomann, R.; Heinzel, T.; Thurn-Albrecht, T. *Colloid. Polym. Sci.* **2004**, *282*, 932. 55.Hong, W. D.; Lam, C. N.; Wang, Y.; He, Y.; Sánchez-Díaz, L. E.; Do, C.; Chen, W.-R. *Phys. Chem. Chem. Phys.* **2019**, *21*, 7745.
- 56.Kuei, B.; Gomez, E. D. Soft Matter 2017, 13, 49.
- 57.Chen, W.-R.; Butler, P. D.; Magid, L. J. *Langmuir* **2006**, *22*, 6539.
- 58.Pal, S.; Nandi, A. K. *J. Appl. Polym. Sci.* **2006**, *101*, 3811.
- 59. Van den Brande, N.; Van Assche, G.; Van Mele, B. *Polymer* **2015**, *57*, 39.
- 60.Yu, L.; Davidson, E.; Sharma, A.; Andersson, M. R.; Segalman, R.; Müller, C. *Chem. Mater.* **2017**, *29*, 5654.
- 61.Martín, J.; Stingelin, N.; Cangialosi, D. *J. Phys. Chem. Lett.* **2018**, *9*, 990.
- 62.Luo, S.; Kui, X.; Xing, E.; Wang, X.; Xue, G.; Schick, C.; Hu, W.; Zhuravlev, E.; Zhou, D. *Macromolecules* **2018**, *51*, 5209.

- 63.Cebe, P.; Partlow, B. P.; Kaplan, D. L.; Wurm, A.; Zhuravlev, E.; Schick, C. *Thermochim. Acta* **2015**, *615*, 8. 64.Balko, J.; Rinscheid, A.; Wurm, A.; Schick, C.; Lohwasser, R. H.; Thelakkat, M.; Thurn-Albrecht, T. *J. Polym. Sci., Part B: Polym. Phys.* **2016**, *54*, 1791.
- 65. Abdelaziz, A.; Zaitsau, D. H.; Mukhametzyanov, T. A.; Solomonov, B. N.; Cebe, P.; Verevkin, S. P.; Schick, C. *Thermochim. Acta* **2017**, *657*, 47. 66. Yagofarov, M. I.; Lapuk, S. E.; Mukhametzyanov, T. A.; Ziganshin, M. A.;
- Schick, C.; Solomonov, B. N. *Thermochim. Acta* **2018**, *668*, 96.
- 67.Pallaka, M. R.; Unruh, D. K.; Simon, S. L. *Thermochim. Acta* **2018**, *663*, 157.
- 68.Malik, S.; Nandi, A. K. *J. Polym. Sci., Part B: Polym. Phys.* **2002**, *40*, 2073.
- 69. Pascui, O. F.; Lohwasser, R.; Sommer, M.; Thelakkat, M.; Thurn-Albrecht, T.; Saalwächter, K. *Macromolecules* **2010**, *43*, 9401.
- 70.Balko, J.; Lohwasser, R. H.; Sommer, M.; Thelakkat, M.; Thurn-Albrecht, T.
- *Macromolecules* **2013**, *46*, 9642.
- 71.Koch, F. P. V.; Heeney, M.; Smith, P. *J. Am. Chem. Soc.* **2013**, *135*, 13699.
- 72. Snyder, C. R.; Nieuwendaal, R. C.;
- DeLongchamp, D. M.; Luscombe, C. K.; Sista, P.; Boyd, S. D. *Macromolecules* **2014**, *47*, 3942. 73.Lee, C. S.; Dadmun, M. D. *Polymer* **2014**, *55*, 4.
- 74.Remy, R.; Weiss, E. D.; Nguyen, N. A.; Wei, S.; Campos, L. M.; Kowalewski, T.; Mackay, M. E. *J. Polym. Sci., Part B: Polym. Phys.* **2014**, *52*, 1469.
- 75. Alizadehaghdam, M.; Heck, B.; Siegenführ, S.; Abbasi, F.; Reiter, G. *Macromolecules* **2019**, *52*, 2487.
- 76.Alizadehaghdam, M.; Siegenführ, S.; Abbasi, F.; Reiter, G. *J. Polym. Sci., Part B: Polym. Phys.* **2019**, *57*, 431.
- 77. Yin, H.; Yang, B.; Chua, Y. Z.; Szymoniak, P.; Carta, M.; Malpass-Evans, R.; McKeown, N. B.; Harrison, W. J.; Budd, P. M.; Schick, C.; Böhning, M.; Schönhals, A. *ACS Macro Lett.* **2019**, *8*, 1022.
- 78.Roland, C. M.; Santangelo, P. G.; Ngai, K. L. *J. Chem. Phys.* **1999**, *111*, 5593.



79.Xie, R.; Lee, Y.; Aplan, M. P.; Caggiano, N. J.; Müller, C.; Colby, R. H.; Gomez, E. D. *Macromolecules* **2017**, *50*, 5146. 80.Koh, Y. P.; Simon, S. L. *Macromolecules* **2013**, *46*, 5815. 81.Gao, S.; Koh, Y. P.; Simon, S. L. *Macromolecules* **2013**, *46*, 562.

82.Xu, J.; Wang, S.; Wang, G.-J. N.; Zhu, C.; Luo, S.; Jin, L.; Gu, X.; Chen, S.; Feig, V. R.; To, J. W. F.; Rondeau-Gagné, S.; Park, J.; Schroeder, B. C.; Lu, C.; Oh, J. Y.; Wang, Y.; Kim, Y.-H.; Yan, H.; Sinclair, R.; Zhou, D.; Xue, G.; Murmann, B.; Linder, C.; Cai, W.; Tok, J. B.-H.; Chung, J. W.; Bao, Z. Science 2017, 355, 59.





GRAPHICAL ABSTRACT

Zhiyuan Qian¹, Luke Galuska¹, William W. McNutt², Michael Ocheje³, Youjun He⁴, Zhiqiang Cao¹, Song Zhang¹, Jie Xu⁵, Kunlun Hong⁴, Renée B. Goodman³, Simon Rondeau-Gagné³, Jianguo Mei², Xiaodan Gu^{1*}

Challenge and solution of characterizing glass transition temperature for conjugated polymers by differential scanning calorimetry

Glass transition temperature (T_g) of conjugated polymers (CPs) cannot be readily measured from DSC. Herein, we measured heat capacity change at $T_{\rm g}$ ($\Delta c_{\rm p}$) for a series of conventional and donor-acceptor (D-A) CPs and compared with polystyrene. Results show a more than one order of magnitude decrease in Δc_p as material changes from flexible and amorphous to rigid and semicrystalline. We also provided a remedy of measuring T_g for D-A CPs with Δc_p of 10^{-3} J·g⁻¹K⁻¹.

GRAPHICAL ABSTRACT FIGURE

